Available online at www.sciencedirect.com
SCIENCE DIRECT®
Combustion and Flame 141 (2005) 40–54
Combustion and Flame
www.elsevier.com/locate/combustflame

Studies of mean and unsteady flow in a swirled combustor using experiments, acoustic analysis, and large eddy simulations

S. Roux [a,*], G. Lartigue [a], T. Poinsot [a,b], U. Meier [c], C. Bérat [d]

[a] *CERFACS, 31057 Toulouse, France*
[b] *IMFT, 31400 Toulouse, France*
[c] *DLR, D-70569 Stuttgart, Germany*
[d] *Turbomeca, 64511 Bordes, France*

Received 14 June 2004; received in revised form 20 September 2004; accepted 22 December 2004

Abstract

The turbulent flow within a complex swirled combustor is studied with compressible large eddy simulation (LES), acoustic analysis, and experiments for both cold and reacting flows. Detailed fields of axial, tangential, and radial velocities (average and RMS) given by LES are compared with experimental values measured by LDV. The unsteady activity is identified using LES and acoustic tools for the whole geometry from inlet (far upstream of the swirler) to the atmosphere (far downstream of the chamber exhaust). Concerning comparisons between experiments and LES, this nose-to-tail procedure removes all ambiguities related to the effects of boundary conditions. Results for the cold flow show that the second acoustic mode at 360 Hz dominates in the plenum while a hydrodynamic mode at 540 Hz due to a precessing vortex core (PVC) is found in the combustion chamber. With combustion, the PVC mode is damped and the main mode frequency dominating all unsteady activity is 500 Hz. Acoustic analysis shows that this mode is still the second acoustic mode observed in the cold flow: its frequency shifts from 360 to 500 Hz when combustion is activated. More generally, these results illustrate the power of combined numerical tools (LES and acoustic analysis) to predict mean flow as well as instabilities in combustors.

Keywords: Gas turbines; Acoustics; Large eddy simulation

1. Introduction

The design of modern combustion chambers for gas turbines relies heavily on Reynolds-averaged Navier–Stokes (RANS), which predicts the mean values of all parameters in the chamber (velocity, temperature, density, species mass fractions, and turbulent quantities). Even though these mean fields are essential ingredients of a successful design, recent research has shown that they had to be complemented by other tools. In the continuous development of gas turbines burners and chambers, unexpected problems such as flashback, quenching, or combustion oscillations appear in many cases. Combustion instabilities are one of the most dangerous phenomena: these oscillations are caused by combustion/acoustics coupling and can

* Corresponding author.
E-mail address: roux@cerfacs.fr (S. Roux).

0010-2180/$ – see front matter
doi:10.1016/j.combustflame.2004.12.007

lead to the complete destruction of the combustor [1–7]. They are difficult to predict at the design level using RANS methods. To understand and predict combustion instabilities, other numerical methods are needed [8,9]:

- Acoustic analysis: using drastic assumptions on the flow and on combustion, the stability of a combustor can be studied using purely acoustic tools which predict the frequency and the growth rates of all modes. Such tools have been used in research centers but also in industry to determine longitudinal low-frequency modes [4,10, 11], longitudinal/azimuthal modes [12,13], fully three-dimensional acoustic modes [12,14], linear or nonlinear dynamics [15–17] with analytical or numerical techniques. The weakest part of these models is the description of the flame response to acoustic perturbations.
- LES: more recently, the development of LES has allowed detailed studies of turbulent combustion. Even though the cost of such LES remains very high, the predictive capacities of these tools for turbulent combustion have been clearly demonstrated [18–21]. Extending LES to study flame/acoustics coupling is therefore an obvious research path [9,22].

Although they can address the same issue (flame/acoustics coupling), acoustic tools and LES follow different routes: while LES provides a detailed analysis of one reacting case, acoustic tools can be used to explore a wide range of parameters and geometries. Combining these solvers is likely to offer the best solution to understand and control combustion oscillations but very few studies have tried to use both approaches together. The objective of this paper is to explore this path by using simultaneously LES and acoustic analysis for a swirled premixed gaseous combustor. These two approaches are compared to detailed measurements performed at DLR Berlin and Stuttgart. First, mean LES profiles are compared for all velocity components (mean and RMS) for cold and reacting flows: this set of data constitutes an extensive validation data base for LES results since it incorporates profiles of mean and RMS velocity components in the axial, tangential, and radial directions. The unsteady activity in the combustor is characterized in a second step using LES, acoustic analysis, and experimental results: the natural hydrodynamic instabilities of the swirled flow (especially the precessing vortex core [23]) are identified and their importance in flow/acoustics coupling is studied for cold and reacting cases. Oscillation frequencies revealed by LES and acoustic analysis are compared to experimental measurements using microphones and hot-wire measurements.

An important aspect of the study is the design of a combustor and the use of numerical tools allowing a 'stand-alone' computation. LES and acoustic analysis are run from an upstream section to the downstream end. Boundary conditions are extremely simple: the mass-flow rate is imposed at the inlet of the whole device while the pressure at infinity is specified far away from the exhaust for the outlet. No boundary condition (like velocity, species, or swirl profiles at the inlet) can be tuned to match results: this allows a more direct evaluation of the two methods' capabilities and limitations.

The experimental configuration is described first before providing short descriptions of the LES and acoustic tools. Results for the nonreacting flow are then presented before results for the reacting case at equivalence ratio 0.75.

2. Configuration: Swirled premixed burner

The burner features a swirled injector (Fig. 1): swirl is produced by tangential injection downstream of a plenum. The chamber has a square cross section (86×86 mm^2) to allow optical diagnostics. The chamber length is 110 mm and ends into an exhaust duct with a 6:1 contraction. The burner operates at atmospheric pressure and the inlet air temperature is 300 K.

In addition to swirl, a central hub is used to stabilize the flame and control its position. In the experiment, methane is injected through holes located in the swirler but mixing is fast so that for the present computations, perfect premixing can be assumed. Experiments include LDV velocity measurements as well as a study of combustion regimes. Velocity profiles are measured for the axial, tangential, and radial components at various sections of the combustor for both cold and reacting flows. Microphones are used to characterize the unsteady activity in the plenum and in the chamber.

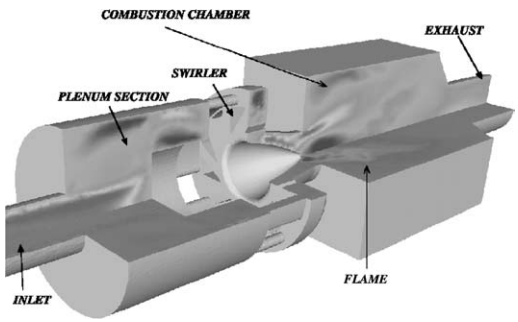

Fig. 1. Global view of the burner and combustion chamber.

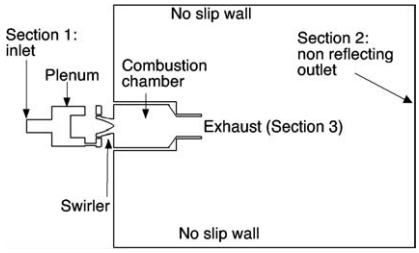

Fig. 2. Boundary conditions: the atmospheric region downstream of the exhaust (Section 3) is also meshed to avoid specifying boundary conditions in this section.

To provide a nonambiguous comparison between LES and experiments, it is important to consider a stand-alone configuration, i.e., a situation where the influence of boundary conditions is as small as possible: for example, the possibility of tuning the LES inlet or outlet conditions to match the experimental results (a procedure which is often employed but rarely mentioned for obvious reasons) must be suppressed. For the present study, boundary conditions were pushed as far away as possible from the chamber by extending the computational domain upstream and downstream of the combustion zone (Fig. 2): the swirlers and the plenum are fully meshed and computed and even a part of the outside atmosphere is meshed to avoid having to specify a boundary condition at the chamber exhaust (Section 3 in Fig. 2). At the inlet of the plenum (Section 1), a flat 27 $\mathrm{m\,s^{-1}}$ velocity profile is imposed ($Re \sim 45{,}000$) and it was checked that this profile had no influence on the results as long as the total mass-flow rate was conserved. The inlet temperature is 300 K. At the outlet of the combustion chamber (Section 3), a part of the exhaust atmosphere is added to the computation. This is an expensive but necessary step: acoustic waves reaching the chamber exhaust (Section 3) are properly transmitted or reflected without having to specify an acoustic impedance for this section since it is not a boundary condition but a part of the computational domain.

3. Large eddy simulations for gas turbines

LES are powerful tools to study the dynamics of turbulent flames [9,20,21,24–27]. In the present article a parallel LES solver called AVBP (see www.cerfacs.fr/cfd/) is used to solve the full compressible Navier Stokes equations on hybrid (structured and unstructured) grids with third-order spatial and temporal accuracy [28,29].

No-slip adiabatic conditions are imposed at all walls of the chamber. Subgrid stresses are described by the WALE model [30]. Even though this model can predict wall turbulence as shown in [30], the mesh size near walls is not sufficient to correctly resolve turbulent boundary layers for all walls of the combustors. This obvious limitation is well known when dealing with LES in combustion chambers but, interestingly, it has limited effects on the results. The comparisons of LES and LDV data show that only a limited zone near the walls is affected by the lack of resolution in these regions: most of the turbulent activity is generated by the velocity gradients inside the chamber which are well resolved on the grid so that this approximation is acceptable. Other simulations performed with law-of-the-walls for LES (not shown in this paper) do not exhibit significant differences with the present no-slip condition.

The flame/turbulence interaction is modeled by the thickened flame/efficiency function model [22,31]. The chemical scheme for methane/air combustion takes into account six species (CH_4, O_2, CO_2, CO, H_2O, and N_2) and two reactions [21].

$$\mathrm{CH_4} + \frac{3}{2}\mathrm{O_2} \rightarrow \mathrm{CO} + 2\mathrm{H_2O}, \tag{1}$$

$$\mathrm{CO} + \frac{1}{2}\mathrm{O_2} \rightleftarrows \mathrm{CO_2}. \tag{2}$$

The first reaction (1) is irreversible whereas the second one (2) is reversible and leads to an equilibrium between CO and CO_2 in the burnt gases and a correct prediction of product temperatures as well as laminar flame speed [21]. The rates of reaction (1) and (2) are respectively given by

$$q_1 = A_1 \left(\frac{\rho Y_{\mathrm{CH_4}}}{W_{\mathrm{CH_4}}}\right)^{n_{1\mathrm{F}}} \left(\frac{\rho Y_{\mathrm{O_2}}}{W_{\mathrm{O_2}}}\right)^{n_{1\mathrm{O}}} \exp\left(-\frac{E_{a1}}{RT}\right), \tag{3}$$

$$q_2 = A_2 \left[\left(\frac{\rho Y_{\mathrm{CO}}}{W_{\mathrm{CO}}}\right)^{n_{2\mathrm{CO}}} \left(\frac{\rho Y_{\mathrm{O_2}}}{W_{\mathrm{O_2}}}\right)^{n_{2\mathrm{O}}} - \left(\frac{\rho Y_{\mathrm{CO_2}}}{W_{\mathrm{CO_2}}}\right)^{n_{2\mathrm{CO_2}}}\right] \exp\left(-\frac{E_{a2}}{RT}\right), \tag{4}$$

where the parameters appearing in these expressions are gathered in Table 1.

Table 1
Rate constants for methane/air two-step scheme

A_1	$n_{1\mathrm{F}}$	$n_{1\mathrm{O}}$	E_{a1}	A_2	$n_{2\mathrm{CO}}$	$n_{2\mathrm{O}}$	$n_{2\mathrm{CO_2}}$	E_{a2}
2×10^{15}	0.9	1.1	35,000	2×10^{9}	1	0.5	1	12,000

Note. The activation energies are in cal/mol and the preexponential constants in cgs units.

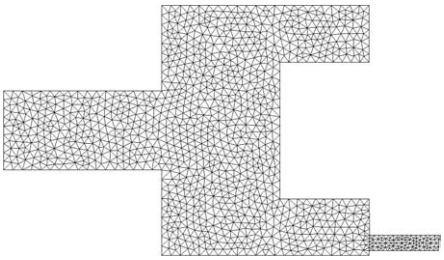

Fig. 3. Mesh resolution in the plenum.

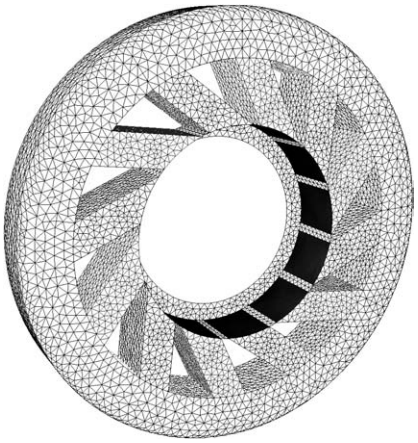

Fig. 4. Mesh resolution in the swirler (12 vanes).

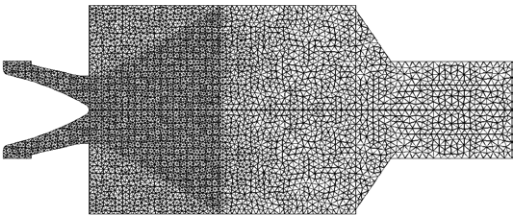

Fig. 5. Mesh resolution in the combustion chamber.

The unstructured mesh used for this study contains 3 million elements. A specific feature of AVBP is the possibility of using hybrid meshes on massively parallel computers: the combustion chamber, the injection, and the exhaust can be computed simultaneously. The distribution of the cells in the computational domain is the same for nonreacting and reacting flow: 20% are located in the plenum (Fig. 3) and in the swirler (Fig. 4), 50% in the upstream half of the combustion chamber, 20% in the downstream half of the combustion chamber (Fig. 5) and 10% in the exhaust pipe and in the atmosphere. Since the solver is fully compressible, acoustic waves are also explicitly captured and characteristic methods are used to specify boundary conditions while controlling acoustic waves reflection [29,32]. For the burner of Fig. 1, the inlet (Section 1 in Fig. 2) is a fixed velocity section while the outlet of the atmosphere part (Section 2) corresponds to a constant pressure surface [9].

In terms of CPU costs, the reduced efficiency (time (μs)/iteration/node) is about 270 for a typically nonreacting computation on one processor. The time step is about 1.5 μs. Computations have been done with an Origin 3000 SGI 500 MHz at the CINES (National Computer Centre for Higher Education: http://www.cines.fr) in Montpelier, France.

4. Three-dimensional acoustic solver

The problem of the coupling between flames and acoustics is old and still unsolved except in certain simple cases. The famous example of the singing flame of Lord Rayleigh [33] demonstrated that this coupling can be very strong: it is sufficient to place a flame in a duct to observe (for certain conditions) that the acoustic modes of the duct can be excited at very high levels. Being able to predict the acoustic eigenmodes of the combustor is therefore a necessary step to understand and avoid combustion instabilities. It was shown in Ref. [34] that the temperature distribution markedly influenced the modal structure and frequencies and that calculations could be carried out with finite element methods. In the present work, a code called AVSP based on the thesis of Nottin [35] is used to solve the Helmholtz equation in a nonisothermal flow [8,9],

$$\nabla \cdot \left(c^2 \nabla p'\right) - \frac{\partial^2}{\partial t^2} p' = 0, \tag{5}$$

where p' is the pressure perturbation and c is the local sound speed. The sound speed c is obtained by averaging LES results. Equation (5) integrates the influence of combustion on the local sound speed but not its effect as an active acoustic generator [9]. This is sufficient to identify modes but not to predict whether they will actually be amplified or damped by the combustor. The pressure fluctuations equation (5) is solved in the frequency domain by assuming harmonic pressure variations at frequency $f = \omega/(2\pi)$,

$$p' = P'(x, y, z) \exp(-i\omega t), \tag{6}$$

with $i^2 = -1$.

Equation (5) then becomes the Helmholtz equation where the unknown quantity is the pressure oscillation amplitude P' at frequency f:

$$\nabla \cdot \left(c^2 \nabla P'\right) + \omega^2 P' = 0. \tag{7}$$

A finite element method is applied to discretize this equation and an eigenvalue solver based on the Arnoldi method is used [36]. Solving Eq. (7) with proper boundary conditions on walls, inlets, and outlets provides the frequencies of the eigenmodes (the

real part of ω), their growth rate (the imaginary part of ω), and the mode structure (the distribution of P'). Like the LES solver, the Helmholtz solver uses hybrid meshes and can be applied to the full geometry of the burner. For the burner considered in the present study (Fig. 1), the acoustic boundary conditions match those used for the LES solver: the inlet (Section 1 in Fig. 2) is treated as a velocity node and the boundary of the atmosphere part meshed for the exhaust (Section 2 in Fig. 2) as a pressure node.

5. Nonreacting flow

The cold flow was characterized for a mass-flow rate of 12 $g\,s^{-1}$. An example of instantaneous axial velocity field is presented in Fig. 6. As expected from the large swirling motion induced by the vanes, a large backflow zone (identified by lines corresponding to zero axial velocity) is found on the chamber axis. Other recirculated zones exist in the corners of the chamber. All these zones are highly unsteady and their position oscillates rapidly with time. Note the complex flow inside the plenum, upstream of the swirler where other recirculated zones are found. Outside Section 3 (Fig. 2), the external atmospheric pressure region is meshed with progressively larger elements to damp perturbations.

5.1. Average profiles

LES and experimental average velocity profiles have been compared at various sections of the combustion chamber (Fig. 7). The averaging time for LES is 100 ms corresponding to 15 flowthrough times in the chamber at the bulk velocity. Data compared for LES and experiments are:

- average axial (Fig. 8), azimuthal (Fig. 10), and radial (Fig. 12) velocities,
- RMS axial (Fig. 9), azimuthal (Fig. 11), and radial (Fig. 13) velocities[1] in the same sections.

A comparison of all profiles shows a good agreement for all velocity components: the mean velocity is correctly predicted as well as the length of the central backflow zone (Fig. 8). The swirl levels observed in the tangential velocity profiles are also good (Fig. 10). Considering that this computation has absolutely no inlet boundary condition which can be tuned to fit the velocity profiles, this confirms the capacity of LES

[1] All RMS quantities are computed with the resolved LES signal. Subgrid scale turbulence effects are not included.

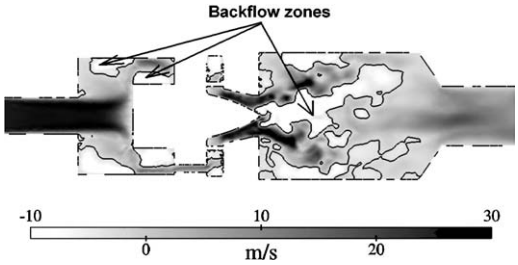

Fig. 6. Instantaneous field of axial velocity for cold flow. The black line corresponds to zero velocity locations.

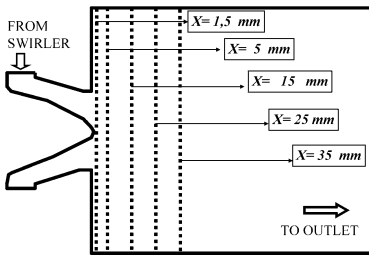

Fig. 7. Section for velocity profiles comparisons.

in such flows. The RMS profiles obtained experimentally by LDV and numerically by LES, for both axial (Fig. 9) and azimuthal (Fig. 11) velocities are also close. The small discrepancies observed close to the chamber axis are due to the experimental difficulty of producing a perfectly symmetric flow: at $x = 5$ mm, for example, the experimental mean profile of tangential velocity (circles in Fig. 10) is not symmetrical and slightly deviates from the LES profiles. Near walls (for $y = -43$ or 43 mm in Figs. 8–13), even though the mesh is not sufficient to resolve turbulent near-wall structures, the agreement for all profiles is good for all available LDV measurements. As mentioned previously, near-wall turbulence has a limited effect on the mean and RMS flow field in the chamber. Table 2 summarizes the quantitative accuracy of the LES prediction. This relies on a comparison between LES and LDV results for the maximum mean/rms axial/tangential/radial velocity (in percentage of their maximum value) and their position (in percentage of the half-width of the combustion chamber).

5.2. Unsteady and acoustic analysis

The RMS fluctuation levels in both LES and experiments (Figs. 9 and 11) are very intense around the axis, close to the inlet of the burner (of the order of 20 m/s at $x = 1.5$ mm). Even though this activity appears as 'turbulence', it is actually due to a large-scale hydrodynamic structure, called precessing vortex core (PVC) which is well known in swirling flows [23,37,38] and is visualized in Fig. 14 from LES data. Sim-

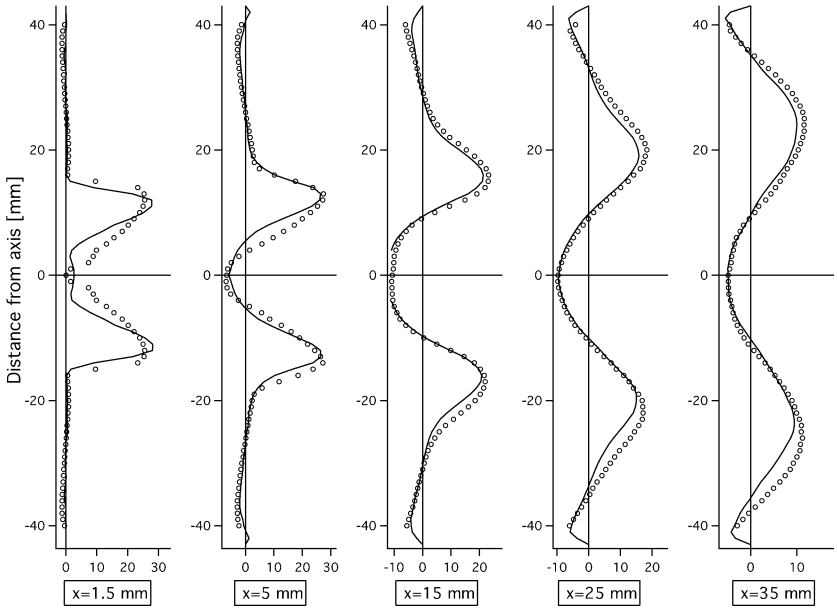

Fig. 8. Average axial velocity profiles for cold flow (○) LDV, (—) LES.

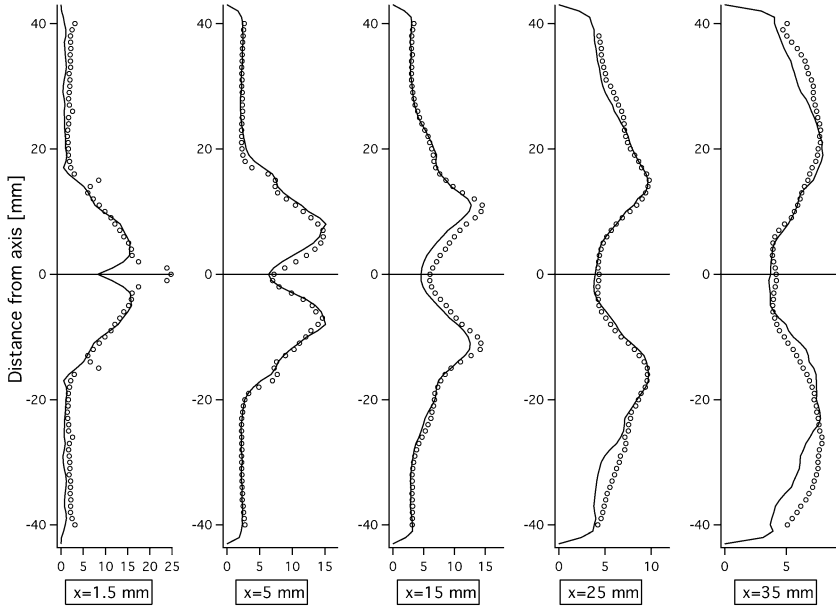

Fig. 9. RMS axial velocity profiles for cold flow. (○) LDV, (—) LES.

ulations indicate that the spiral structure appearing in Fig. 14 rotates around the burner axis at a frequency of 540 Hz. Measurements performed inside the chamber reveal a dominant frequency around 510 Hz.

The Helmholtz solver confirms the hydrodynamic nature of the 540 Hz frequency which does not appear as an acoustic eigenmode: the acoustic modes of the combustor obtained with AVSP are listed in Table 3 and none of them matches the 540 Hz frequency. The first acoustic mode of Table 3 (172 Hz) is not observed in LES nor in experiments: this mode is stable. However, the second mode (363 Hz) is indeed identified in experiments (around 340 Hz) and in LES (around 360 Hz) but only in the plenum and in the exhaust pipe. This mode is actually present everywhere in the device but it is dominated by the PVC signal inside the first part of the chamber. Fig. 15 shows experimental and numerical pressure spectra measured

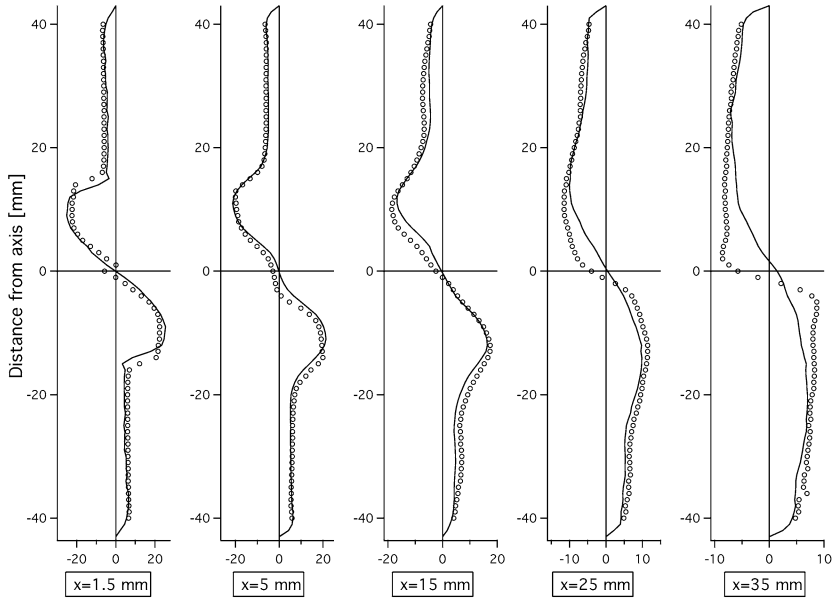

Fig. 10. Average azimuthal velocity profiles for cold flow. (○) LDV, (—) LES.

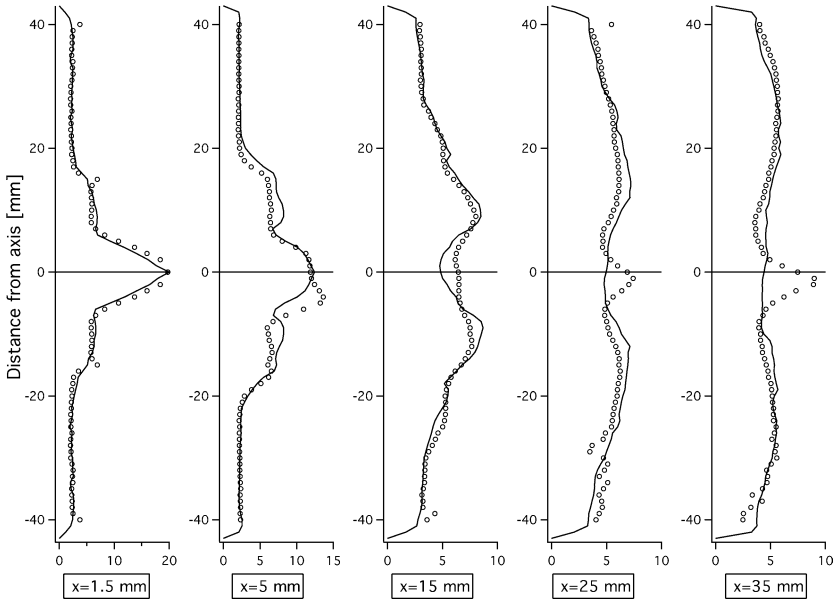

Fig. 11. RMS azimuthal velocity profiles for cold flow. (○) LDV, (—) LES.

in the plenum and in the chamber and confirms that these two modes exist simultaneously but not in the same places.

To extend the analysis of these modes and especially to look at their spatial structure, it is not easy to use measurements since they would require multiple simultaneous pressure probes. It is more convenient to rely on LES and acoustic calculations: the pressure fluctuations amplitude (measured by $\overline{p'^2}^{1/2}$) computed both with LES and with the acoustic solver are presented in Fig. 16. Since the 3/4 wave mode has a long wavelength compared to the chamber, this plot is obtained in the LES and in the Helmholtz solver by displaying local RMS pressure versus x coordinate. In Fig. 16, LES shows RMS of the whole pressure signal whereas the acoustic solver displays only the RMS acoustic structure of the 363 Hz mode. The two codes give similar pressure amplitudes in the plenum

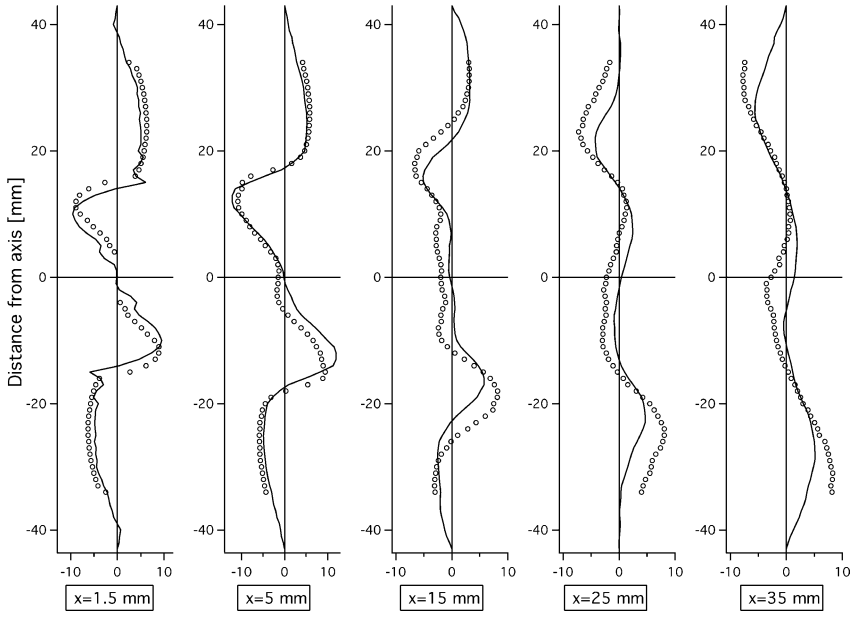

Fig. 12. Average radial velocity profiles for cold flow. (○) LDV, (—) LES.

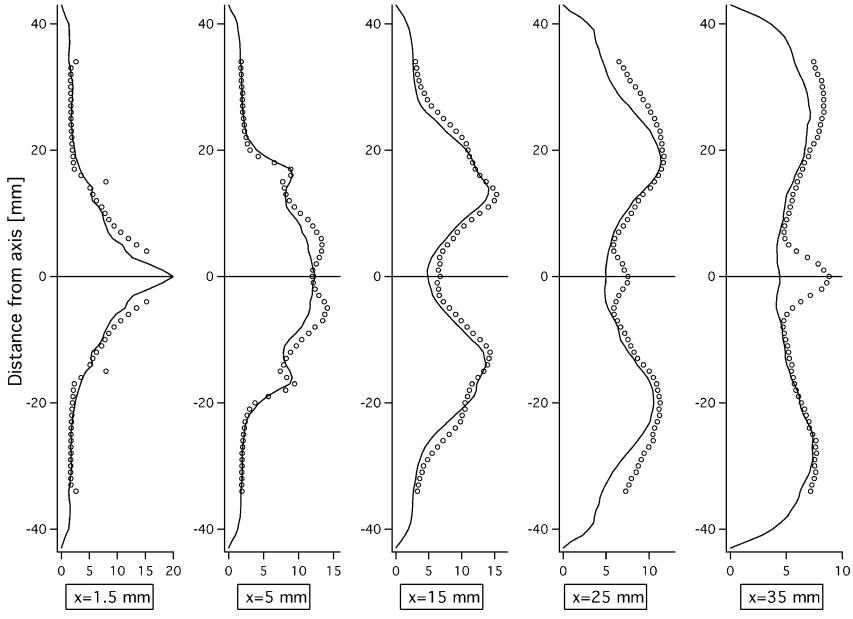

Fig. 13. RMS radial velocity profiles for cold flow. (○) LDV, (—) LES.

Table 2
Longitudinal modes frequencies predicted by Helmholtz solver (Helm), measured in the experiment (Exp) and in the LES (LES)

Mode number	Mode name	Cold flow (Hz)			Reacting flow (Hz)		
		Helm	Exp	LES	Helm	Exp	LES
(1)	1/4 wave	172	damped	damped	265	300	290
(2)	3/4 wave	363	340	360	588	570	500
(3)	5/4 wave	1409	damped	damped	1440	damped	damped

Table 3
Accuracy of the LES/experiment comparison for nonreacting case

	Mean velocity			RMS velocity		
	Axial	Tangential	Radial	Axial	Tangential	Radial
Max. value	10%	8%	30%	4%	no isolated max.	8%
Max. value position	1%	2%	2%	3%	no isolated max.	5%

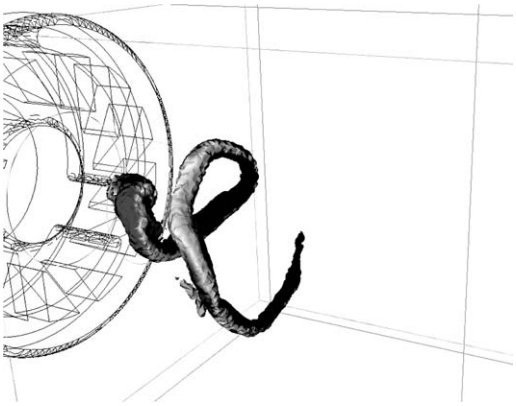

Fig. 14. Visualization of the 540 Hz PVC hydrodynamic instability at the exit of the swirler using an isosurface of low pressure.

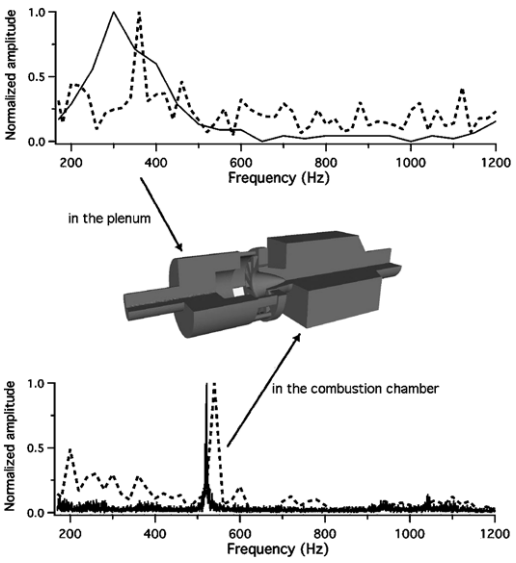

Fig. 15. Pressure fluctuations spectra for cold flow at two locations. Solid line, experiment; dashed line, LES.

($x < -0.05$ m) and in the exhaust ($x > 0.05$ m), indicating the acoustic nature of the pressure fluctuations in these regions. However, in the swirler and in the first half of the chamber (-0.05 m $< x < 0.05$ m), the pressure fluctuations given by LES are larger than the acoustic predictions of the Helmholtz solver: these fluctuations are due to the PVC at 540 Hz. The PVC

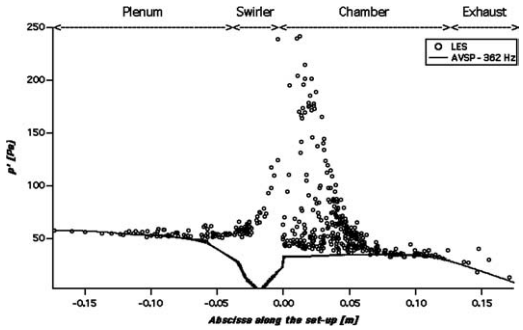

Fig. 16. Pressure fluctuations amplitude obtained by LES (circles) and acoustic analysis (solid line) code for cold flow.

acts acoustically like a rotating solid placed in the flow: this dipole radiates weakly outside of the chamber. This explains why the acoustic mode at 360 Hz is visible and unaffected in the plenum and in the exhaust.

High levels of RMS velocity are found also in the swirler (not shown here) confirming the requirement for an entrance to exhaust computation: there is no section in the swirler or in the chamber inlet which could possibly be used to specify inlet boundary conditions and reduce the size of the computational domain.

In summary, for cold flow, two modes coexist: a low-amplitude acoustic (3/4 wave) mode at 360 Hz everywhere in the device and a strong hydrodynamic mode at 540 Hz due to the PVC, localized near the burner inlet ($0 < x < 5$ cm).

6. Reacting flow

The reacting case corresponds to an equivalence ratio of 0.75, an air flow rate of 12 g/s, and a thermal power of 27 kW. A snapshot of an instantaneous temperature isosurface (Fig. 17) reveals a compact flame located close to the burner inlet. Fig. 18 shows the pseudo-streamline pattern on the x–r plane based on the mean axial and radial velocity components. A central toroidal recirculation zone is established in the wake of the center body under the effect of the swirling flow. A corner recirculation zone is formed downstream of the backward-facing step.

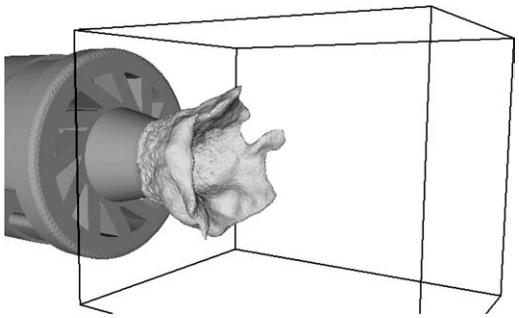

Fig. 17. Instantaneous 1250 K isosurface (LES data).

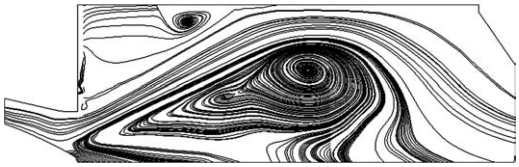

Fig. 18. Mean x–r pseudo-streamline pattern.

6.1. *Average profiles*

Mean and RMS temperature profiles are displayed in Fig. 19. As expected from the snapshot of Fig. 17, combustion is nearly finished at $x = 35$ mm and no fresh gases are found (in the mean) beyond this section. RMS temperature levels are quite high close to the burner inlet (300 K), indicating a strong intermittency and flame flapping in this zone. No comparison is possible with experiments here because temperatures have not been measured yet.

The velocity fields, however, have been measured and are presented in Figs. 20 (mean axial), 21 (RMS axial), 22 (mean tangential), 23 (RMS tangential), 24 (mean radial), 25 (RMS radial). The overall agreement between mean LES results and experimental data is good. Table 4 gives an overview of the quantitative accuracy of the LES prediction. It is based on a comparison between LES and LDV results in terms of the maximum mean/rms axial/tangential/radial velocity (in percentage of their maximum value) and their position (in percentage of the half-width of the combustion chamber). The rather low accuracy of the RMS maximum values may come from the fact that the subgrid-scale fluctuations are not included in the RMS values shown in the present paper.

The LES captures both the mean values and the fluctuations precisely, except in a zone close to the burner inlet. This lack of precision could be due to an insufficient mesh resolution in this region but a more fundamental issue linked to averaging techniques in nonconstant density flows is probably responsible for the discrepancy observed in these regions: LES averages are obtained using time averages of the Favre-filtered LES quantities while the averaging process (Favre or Reynolds) used for experimental results (LDV measurements) is often difficult to qualify because of data sampling [9,39]. Most zones where experiments and LES do not match in Figs. 21 or 23 are regions where the RMS temperature (Fig. 19) is large, i.e., zones with strong intermittency. In these regions,

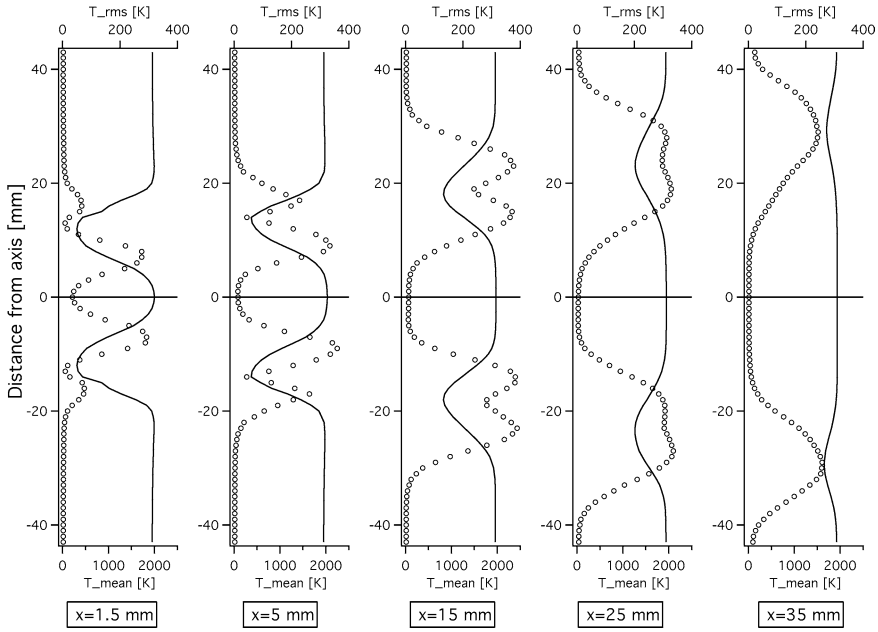

Fig. 19. Mean (solid line) and RMS (circles) temperature in the central plane of the combustor (LES data).

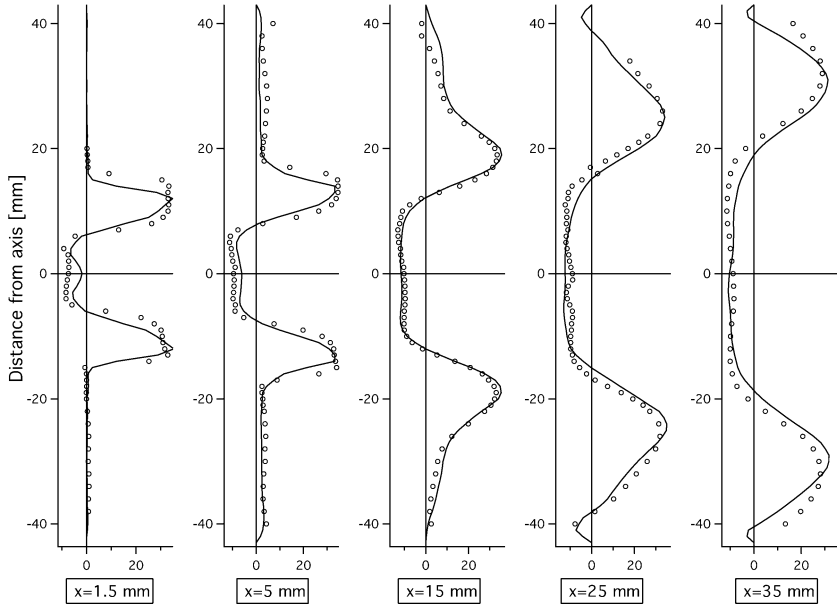

Fig. 20. Mean axial velocity in the central plane for reacting flow. (○) LDV, (—) LES.

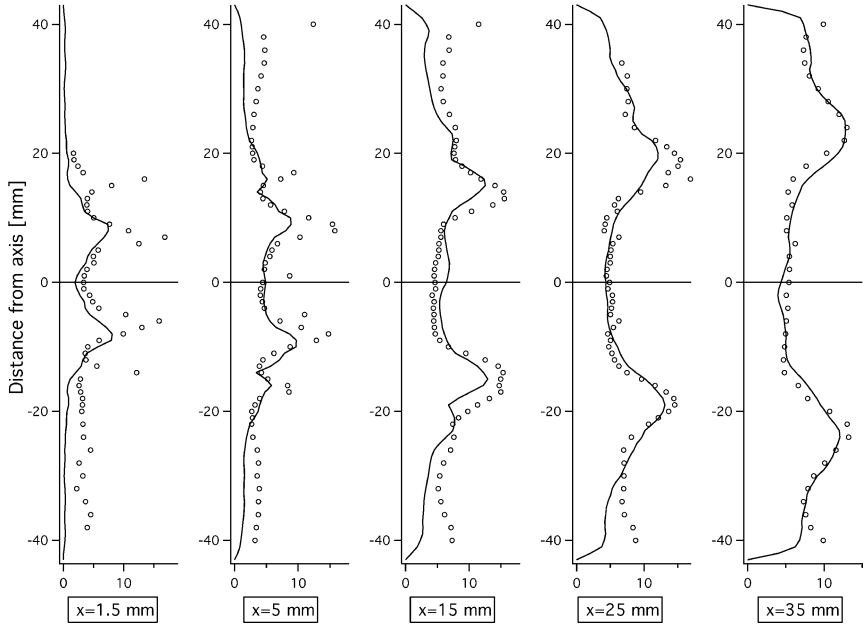

Fig. 21. RMS axial velocity in the central plane for reacting flow (○) LDV, (—) LES.

Table 4
Accuracy of the LES/experiment comparison for reacting case

	Mean velocity			RMS velocity		
	Axial	Tangential	Radial	Axial	Tangential	Radial
Max. value	6%	5%	11%	33%	16%	19%
Max. value position	1%	3%	5%	7%	8%	0%

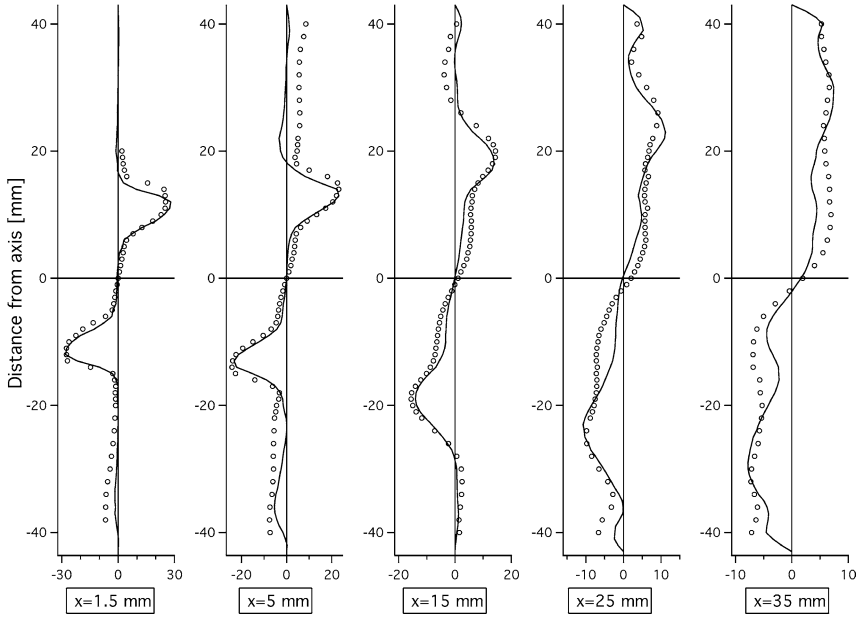

Fig. 22. Mean tangential velocity in central plane for reacting flow. (○) LDV, (—) LES.

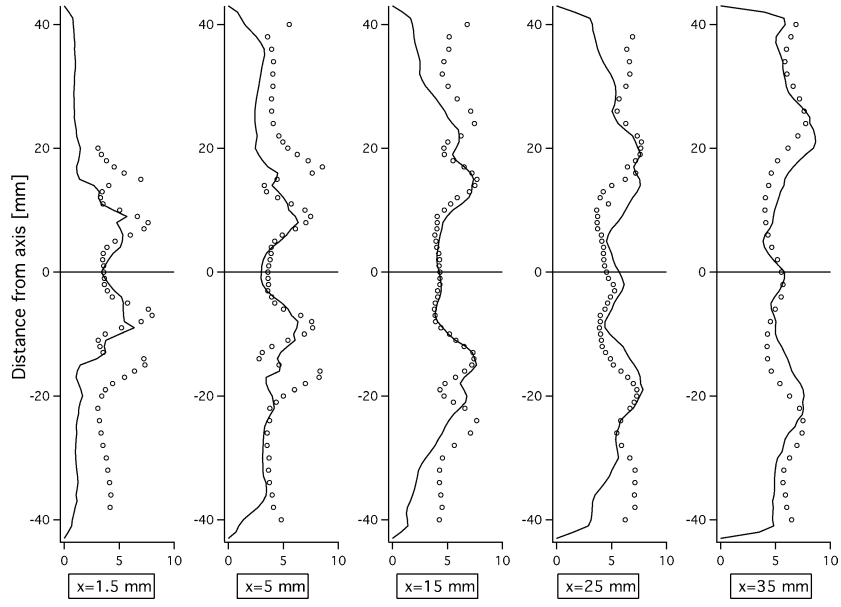

Fig. 23. RMS tangential velocity in central plane for reacting flow. (○) LDV, (—) LES.

Reynolds and Favre averages can be very different [9] and this could be the source of the present errors. In regions with limited RMS temperatures (for example, at $x = 35$ mm), the experimental and LES data match very well, confirming the possible explanation. Obviously, these results suggest that more studies are required to clarify this issue and this is left for further work.

6.2. Unsteady and acoustic analysis

The first major consequence of combustion is to damp the PVC observed under cold-flow conditions. Even though this mechanism cannot be expected to exist in all swirled combustors, it has already been observed in other cases [21]. With combustion, dilatation and increased viscosity in the burnt gases seem to

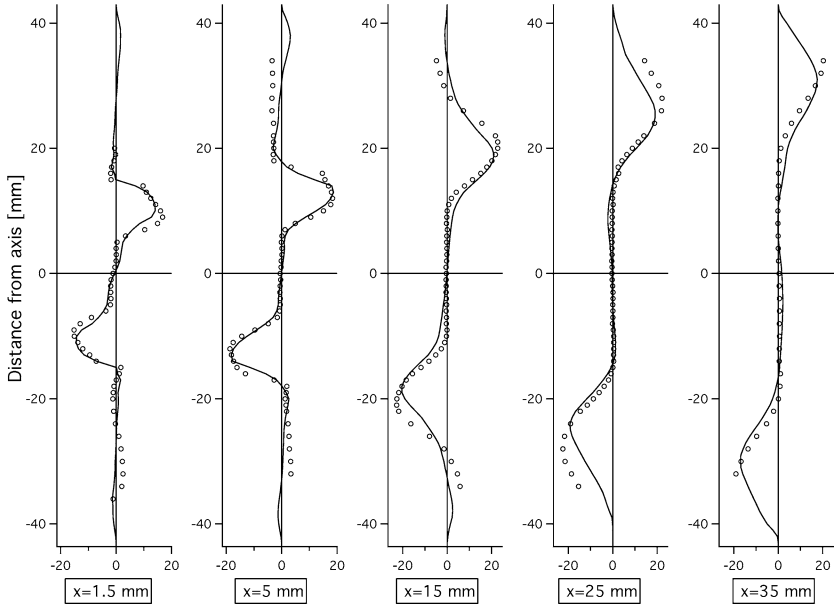

Fig. 24. Mean radial velocity in central plane for reacting flow. (○) LDV, (—) LES.

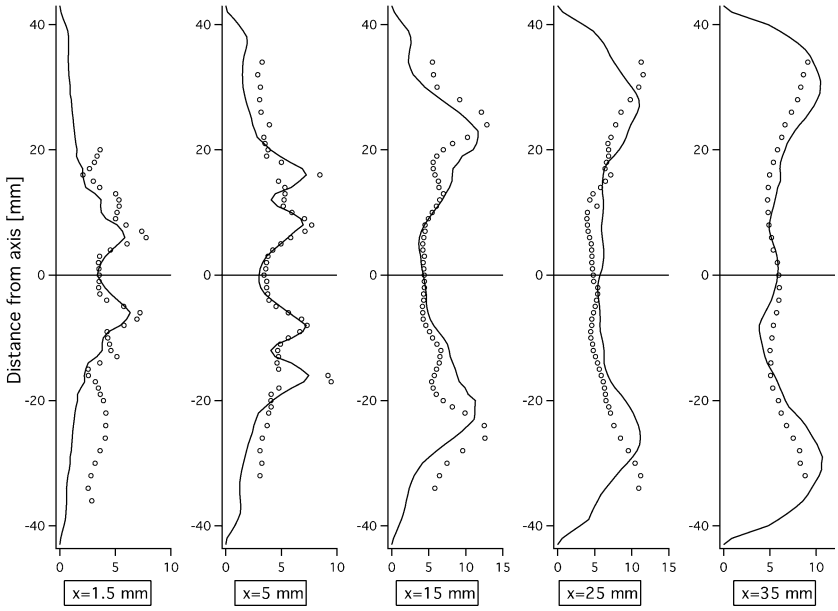

Fig. 25. RMS radial velocity in central plane for reacting flow. (○) LDV, (—) LES.

damp the PVC: its signature on the unsteady pressure field disappears and is replaced by the acoustic mode traces.

For this reacting flow, two self-excited acoustic modes appear experimentally around 300 Hz and 570 Hz. To identify the nature of these modes, the Helmholtz solver was run using the average temperature field given by LES to obtain the list of acoustic eigenmodes with combustion. Table 3 confirms that the two frequencies observed in experiments correspond to the first two modes (1/4 wave and 3/4 wave) of the combustor. The agreement between measurements and the Helmholtz solver is quite good: around 10% for the 1/4 wave and less than 2% for the 3/4 wave mode. The most amplified mode is still the 3/4 wave mode which was already observed for the cold flow: its frequency shifted from 360 Hz (cold flow) to 570 Hz (reacting flow). The difference between the

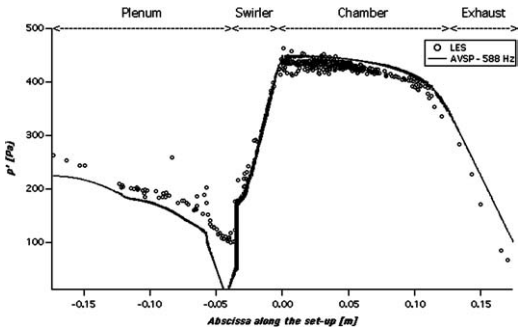

Fig. 26. Pressure fluctuations amplitude predicted by the LES code (circles) and the acoustic solver (line) for reacting flow.

measured LES frequency (500 Hz) and the experimental (570 Hz) or Helmholtz solver (588 Hz) values for this mode is probably due to changes in acoustic boundary conditions but there is little doubt that LES, experiments, and Helmholtz solver are pointing at the same mode: this can be checked by displaying the field of RMS pressure measured in the LES along the chamber axis together with the modal structure predicted by the Helmholtz solver for the 3/4 wave mode (Fig. 26). Even though the LES signal contains the signature of all modes (and not only of the 3/4 wave mode), its shape neatly matches the structure of the 3/4 wave mode predicted by the Helmholtz solver. Unlike the RMS pressure profile for the cold flow (Fig. 16), the match between the LES and the Helmholtz solver is good everywhere, even in the combustion chamber, indicating that the whole flow is locked on the 3/4 wave mode.

In summary, with combustion (for this regime at an equivalence ratio of 0.75), the hydrodynamic mode (PVC) is damped and the acoustic level is enhanced. The most amplified mode is the 3/4 wave mode for the whole device (Fig. 26). The mode structure measured in the LES matches the structure predicted by the Helmholtz code.

7. Conclusions

LES and acoustic analysis were used jointly to analyze a swirled premixed combustor and the results were compared to experimental data. Both the mean flow and the unsteady activity were studied for cold and reacting regimes. The full geometry was computed from plenum inlet to atmosphere to avoid any possible bias effect or tuning exercises of boundary conditions during LES/experiments comparison.

The mean values of velocity measured in five sections in the chamber obtained with LES closely match experimental data for both cold flow and for a reacting case at an equivalence ratio of 0.75. The RMS values are also in good agreement for the cold flow with limited differences for reacting flows in regions of large intermittency, suggesting that these errors might be due to the definition of the averaging procedure in these regions (Favre vs Reynolds). Generally speaking, these results confirm the remarkable predictive capacity of LES methods and also highlight the need for well-defined boundary conditions: for example, the computation must include the swirler vanes and cannot start at the chamber inlet plane.

Regarding the unsteady behavior of the flow the LES results (confirmed by experimental data) show that, without combustion, the 3/4 wave acoustic longitudinal mode at 360 Hz coexists with a precessing vortex core at 540 Hz. With combustion, the pressure fluctuations in the chamber lock onto the 3/4 wave acoustic mode of the device which shifts from 360 Hz (cold flow) to 588 Hz (reacting case): the PVC disappears and the acoustic structure revealed by LES matches exactly the prediction of the acoustic solver for this mode. Future studies will concentrate on the unsteady flame motion using PLIF and Raman measurements but the present results demonstrate that the nature of the acoustic/flow coupling changes when combustion is activated: hydrodynamic structures such as PVC appearing in cold flow can disappear when combustion starts while acoustic modes are reinforced by combustion. More generally, this study confirms the potential of LES for such flows and also highlights the need for Helmholtz solvers and a joint use of both methods.

Acknowledgments

The support of Turbomeca and of the EC project PRECCINSTA is gratefully acknowledged. This work has been carried within the framework of the PRECCINSTA project, section Thermoacoustic Interaction Fundamentals (WP2), of the European Union (EU Contract ENK5-CT-2000-00060). The support of CINES is also gratefully acknowledged.

References

[1] B.D. Mugridge, J. Sound Vibration 70 (1980) 437–452.
[2] T. Poinsot, A. Trouvé, D. Veynante, S. Candel, E. Esposito, J. Fluid Mech. 177 (1987) 265–292.
[3] M.A. Macquisten, A.P. Dowling, Combust. Flame 94 (1994) 253–264.
[4] A.P. Dowling, J. Fluid Mech. 346 (1997) 271–290.
[5] T. Lieuwen, B.T. Zinn, Proc. Combust. Inst. 27 (1998) 1809–1816.
[6] W. Krebs, P. Flohr, B. Prade, S. Hoffmann, Combust. Sci. Technol. 174 (2002) 99–128.

[7] S. Candel, Proc. Combust. Inst. 29 (2002) 1–28.
[8] D.G. Crighton, A. Dowling, J.F. Williams, M. Heckl, F. Leppington, Modern Methods in Analytical Acoustics, Springer-Verlag, New York, 1992.
[9] T. Poinsot, D. Veynante, Theoretical and Numerical Combustion, Edwards, 2001.
[10] T. Lieuwen, B.T. Zinn, J. Sound Vibration 235 (2000) 405–414.
[11] C.O. Paschereit, W. Polifke, B. Schuermans, O. Mattson, J. Eng. Gas Turb. Power 124 (2002) 239–247.
[12] G. Walz, W. Krebs, S. Hoffmann, H. Judith, in: Proc. Int. Gas Turbine and Aeroengine Congress and Exhibition, 1999.
[13] S.R. Stow, A.P. Dowling, Proc. ASME Paper 2003-GT-38168, 2003.
[14] S. Zikikout, S. Candel, T. Poinsot, A. Trouvé, E. Esposito, Proc. Combust. Inst. 21 (1986) 1427–1434.
[15] F.E.C. Culick, Astronautica Acta 3 (1976) 714–757.
[16] T. Poinsot, S. Candel, Combust. Sci. Technol. 61 (1988) 121–153.
[17] F.E.C. Culick, AIAA J. 32 (1994) 146–169.
[18] H. Forkel, J. Janicka, Flow Turb. Combust. 65 (2000) 163–175.
[19] Y. Huang, H.G. Sung, S.Y. Hsieh, V. Yang, J. Prop. Power 19 (2003) 782–794.
[20] C.D. Pierce, P. Moin, J. Fluid Mech. 504 (2004) 73–97.
[21] L. Selle, G. Lartigue, T. Poinsot, R. Koch, K.-U. Schildmacher, W. Krebs, B. Prade, P. Kaufmann, D. Veynante, Combust. Flame 137 (2004) 489–505.
[22] C. Angelberger, F. Egolfopoulos, D. Veynante, Flow Turb. Combust. 65 (2000) 205–222.
[23] O. Lucca-Negro, T. O'Doherty, Prog. Energy Combust. Sci. 27 (2001) 431–481.
[24] P.E. Desjardins, S.H. Frankel, Combust. Flame 119 (1999) 121–133.
[25] D. Caraeni, C. Bergström, L. Fuchs, Flow Turb. Combust. 65 (2000) 223–244.
[26] N. Peters, Turbulent Combustion, Cambridge Univ. Press, 2000.
[27] H. Pitsch, L. Duchamp de la Geneste, Proc. Combust. Inst. 29 (2002) 2001–2005.
[28] O. Colin, M. Rudgyard, J. Comput. Phys. 162 (2000) 338–371.
[29] V. Moureau, G. Lartigue, Y. Sommerer, C. Angelberger, O. Colin, T. Poinsot, J. Comput. Phys. (2004), in press.
[30] F. Nicoud, F. Ducros, Flow Turb. Combust. 62 (1999) 183–200.
[31] O. Colin, F. Ducros, D. Veynante, T. Poinsot, Phys. Fluids 12 (2000) 1843–1863.
[32] L. Selle, F. Nicoud, T. Poinsot, AIAA J. 42 (2004) 958–964.
[33] L. Rayleigh, Nature July 18 (1878) 319–321.
[34] A.M. Laverdant, T. Poinsot, S. Candel, J. Prop. Power 2 (1986) 311–316.
[35] C. Nottin, Ph.D. thesis, Ecole Centrale Paris, 2002.
[36] R. Lehoucq, D. Sorensen, ARPACK User's Guide: Solution of Large Scale Eigenvalue Problem with Implicitly Restarted Arnoldi Methods, 1997.
[37] M.G. Hall, Annu. Rev. Fluid Mech. 4 (1972), 195–217.
[38] P. Billant, J.-M. Chomaz, P. Huerre, J. Fluid Mech. 376 (1998) 183–219.
[39] C. Chen, J.J. Riley, P. McMurtry, Combust. Flame 87 (1991) 257–277.